7. SEDIMENTARY PROCESSES OF VOLCANICLASTIC SEDIMENTS, LEG 136[1]

Jiro Naka,[2] Ryosuke Tsugaru,[3] Tohru Danhara,[4] Takeo Tanaka,[2] and Kantaro Fujioka[2]

ABSTRACT

Sediment cores recovered from three holes drilled during Ocean Drilling Program Leg 136 include volcaniclastics probably derived from the Hawaiian islands. The volcaniclastics shallower than 10 meters below seafloor are fresh and are composed of basaltic glass (sideromelane), basaltic fragments (mainly tachylite), plagioclase, olivine, pyroxene, and opaque minerals. Most of these glasses are probably products of hydrovolcanism. Visibly, some of these volcaniclastics are recognized as bedded ash layers having thicknesses that range from 5 to 10 cm. However, many volcaniclastics are disrupted by bioturbation to some degree, and are sometimes totally mixed with ambient brown clays. No visible correlative ash layer among these holes was found. It seems that many ash layers thinner than the bedded layers were disrupted by bioturbation because of the low sedimentation rate of volcaniclastics.

The volcaniclastics were probably transported one of two ways: through air fall and pelagic settling or through turbidity-current transport. Other archipelagic apron volcaniclastic sediments of volcanic seamounts suggest that turbidite transport is the favored explanation of origin.

INTRODUCTION

During Ocean Drilling Program (ODP) Leg 136, sediment cores were collected at Holes 842A, 842B, and 843C, 220 km from the island of Oahu (Figs. 1 and 2), in the southern outer area of the Hawaiian Arch (Hamilton, 1957) and archipelagic apron. These holes are on the crest of a small ridge-like knoll that has low elevation and gentle slope (Dziewonski, Wilkens, Firth, et al., 1992). Therefore, it seems the contribution of detrital sediments from the Hawaiian Islands is minimal.

Distances between these three holes are less than 1000 m; the distance between Holes 842A and 842B is a few tens of meters. Therefore, the major lithology among these holes is similar (brown clayey silt and silty clay) and includes volcaniclastics (ash) as the minor lithology. The origin of the upper part of these volcaniclastics could be referred to as volcanism from the Hawaiian Islands (Garcia, this volume). However, the amounts and occurrences of volcaniclastics are different. In this report, sedimentological features of these volcaniclastic sediments are described, and the possible deposition processes of these ash layers are discussed.

METHODS

Composition of the sediments was determined from smear slides for 42 samples and thin sections for 20 samples. The shapes of coarse fractions of these sediments were observed by scanning electron microscopy (SEM).

Grain-size distributions for 42 samples were determined using a Shimazu Co. Ltd. Model SALD-1100 laser-beam particle-size analyzer after removal by suspension in distilled water, agitation in an ultrasonic cleaner, and decantation. The length and width of volcaniclastic fragments were measured in thin section for Samples 136-842A-1H-6, 58–59 cm, and -1H-6, 67–68 cm.

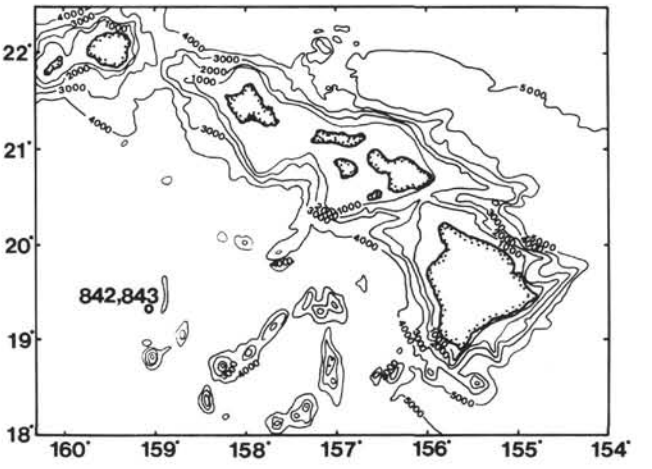

Figure 1. Location map of Sites 842 and 843. Bathymetry in meters.

Reflective indices of basaltic glass shards from the sediments were measured with the Reflective Index Measurement System Model RIMS-86 of Kyoto Fission Track Co. Ltd., using the experimental procedures of Danhara et al. (1992). The accuracy of the reflective index for a single shard is better than 99.99%.

RESULTS

Brief Description of Sampling

Figure 3 shows the location of the discrete ash layer and the relative abundance of dispersed ash in cores from these three holes. These discrete ash layers include visibly well-preserved, moderately bioturbated, and heavily bioturbated ash layers. Samples were collected from some of these layers and from some homogeneous parts as background. Interval 136-842A-1H-6, 63–70 cm, has well-preserved ash layers (Fig. 4A). The bottom of these layers shows a sharp surface. However, the layers are mottled and mixed with pelagic brown clay toward the top. Visibly normal grading is the only internal sedimentary structure, and there are three upward-fining sequences within this interval. We observed some coarse-grained concentrated wavy bands microscopically, but the boundary between surrounding areas is not clear (probably disturbed by bioturbation).

[1] Wilkens, R.H., Firth, J., Bender, J., et al., 1993. *Proc. ODP, Sci. Results*, 136: College Station, TX (Ocean Drilling Program).

[2] JAMSTEC, 2-15 Natsushima-cho, Yokosuka 237, Japan.

[3] Ocean Research Institute, University of Tokyo, 1-15-1 Minamidai, Nakano-ku, Tokyo 164, Japan (Current address: Inter Science Co. Ltd., 1-5-9 Toranomon, Minato-ku, Tokyo 105, Japan).

[4] Kyoto Fission Track Co., Ltd., Umezu Kita-machi 33, Ukyu-ku, Kyoto 615, Japan.

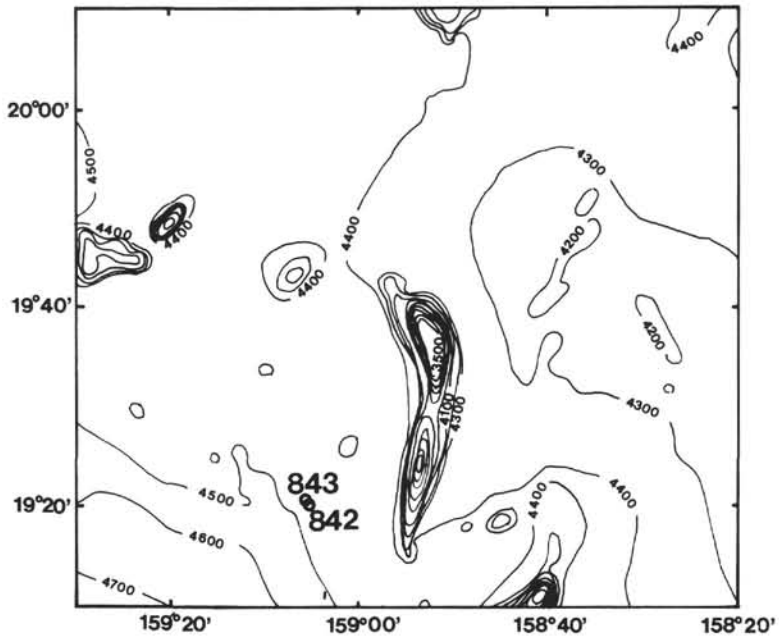

Figure 2. Detailed bathymetry (in meters) around Sites 842 and 843 (after Brocher and ten Brink, 1987).

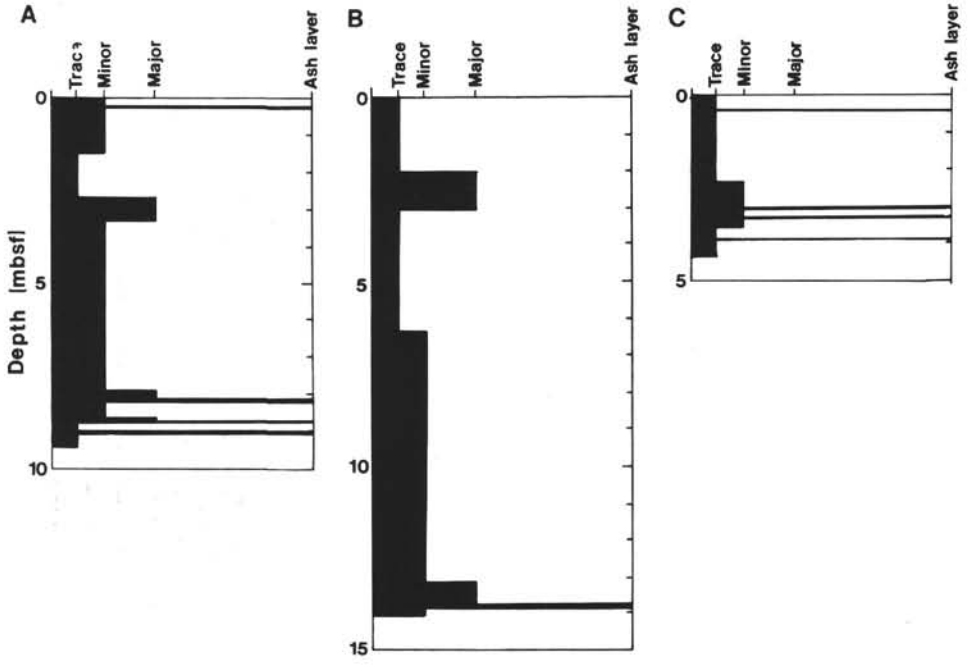

Figure 3. Location of ash layers and relative abundance of dispersed ash with depth in Cores 136-842A-1H (**A**), 136-842B-1H and -2H (**B**), and 136-843C-1H (**C**) (modified from Dziewonski, Wilkens, Firth, et al., 1992).

An ash layer between Interval 136-842A-1H-6, 120–126 cm, is moderately disturbed by bioturbation, although an upward-fining sequence is observed within it (Fig. 4B). The bottom surface is heavily undulated, but the contact with clay underneath is sharp, and beneath this bottom surface there are some small pods filled by sand-size volcaniclastics existing within nannofossil ooze (Pl. 1, Fig. 4).

Some visible ash layers were recovered from Hole 842B, but most of the volcanic glasses are altered. Visible ash layers from Hole 843C are all disrupted by bioturbation.

SEM, Smear Slide, and Thin-Section Observations

The results of a point count of thin sections are shown in Table 1. In each hole, 842A, 842B, and 843C, fresh glass (sideromelane) shards (Pl. 1, Figs. 1, 2, 4) are well-preserved in depths shallower than 10 mbsf. These glass shards show some angular varieties. The most dominant type is the blocky shaped type 1 of Wohletz (1983); other varieties observed are type 2, 3, and 4 of Wohletz (1983) and scoria (Pls. 2 and 3). The other volcaniclastic materials are tachylite (now opaque), pla-

Table 1. Modal compositions of sediments of Hole 842A and 842B (in percent).

Sample (cm)	842A-1H-1, 20–21	842A-1H-6, 42–43	842A-1H-6, 58–59	842A-1H-6, 67–68	842A-1H-6, 71–72	842A-1H-1, 119–120	842A-1H-6, 123–124	842A-1H-6, 127–128	842B-1H-1, 20–21	842B-1H-2, 19–20
Glass[a]	6.4	1.3	4.5	13.6	1.8	3.7	8.0	0.8	1.5	4.7
Altered glass[b]	0.1	0.4	1.3	2.3	0.3	1.3	0.9	0.4	0.1	0.3
Basaltic fragments[c]	1.0	1.0	3.2	13.5	0.3	2.4	5.4	0.0	1.0	0.9
Plagioclase	1.0	3.2	6.4	11.5	0.6	5.1	5.9	0.6	1.9	1.7
Olivine	0.3	1.2	2.1	5.4	0.4	1.6	1.8	0.2	1.5	0.8
Pyroxene	0.1	0.2	0.4	3.5	0.0	0.4	0.5	0.0	0.4	0.0
Opaque minerals[d]	6.2	5.4	6.8	8.6	3.3	3.3	4.5	3.5	3.7	4.3
Siliceous fossils[e]	8.3	2.8	0.6	2.5	6.9	2.0	1.6	7.0	0.3	8.6
Calcareous fossils[f]	0.0	0.0	0.0	0.0	0.0	0.0	0.2	0.3	0.0	0.0
Clay[g]	76.6	84.5	74.7	39.1	86.4	80.2	71.2	87.2	89.6	79.7

Sample (cm)	842B-1H-2, 99–100	842B-1H-3, 19–20	842B-1H-4, 20–21	842B-1H-4, 98–99	842B-2H-2, 98–99	842B-2H-3, 65–66	842B-2H-4, 2–3	842B-2H-5, 75–76	842B-2H-5, 88–89	842B-2H-5, 96–97
Glass[a]	14.8	0.5	1.7	1.8	0.8	1.4	0.5	0.0	0.1	0.0
Altered glass[b]	0.2	0.5	0.3	0.1	0.5	0.8	0.5	0.5	13.9	0.6
Basaltic fragments[c]	4.4	0.9	1.8	1.6	1.0	2.7	3.2	1.0	13.6	1.6
Plagioclase	1.2	1.6	1.3	1.3	2.3	2.1	3.1	1.1	4.3	1.7
Olivine	0.5	0.4	0.9	0.7	0.3	0.9	1.0	0.2	2.7	0.1
Pyroxene	0.1	0.2	0.0	0.0	0.2	0.2	0.2	0.0	0.3	0.4
Opaque minerals[d]	5.4	4.7	4.0	5.2	2.9	5.8	5.3	1.7	5.8	3.6
Siliceous fossils[e]	9.4	0.0	0.6	6.2	0.2	0.1	0.0	0.4	0.4	0.1
Calcareous fossils[f]	0.0	0.0	0.0	0.0	0.0	0.0	0.0	0.0	0.0	0.0
Clay[g]	64.0	91.2	89.4	83.1	91.8	86.0	86.2	95.1	58.9	91.9

Note: Based on 1000-point count on thin section.
[a] Fresh sideromelane.
[b] Mostly altered to clay minerals.
[c] Sideromelane or tachylite including crystals.
[d] Mostly tachylite and minor amounts of "red brown semiopaque oxides."
[e] Mostly radiolarians and diatoms and minor amounts of sponge spicules and silicoflagellates.
[f] Foraminifers.
[g] Particles smaller than 15 μm.

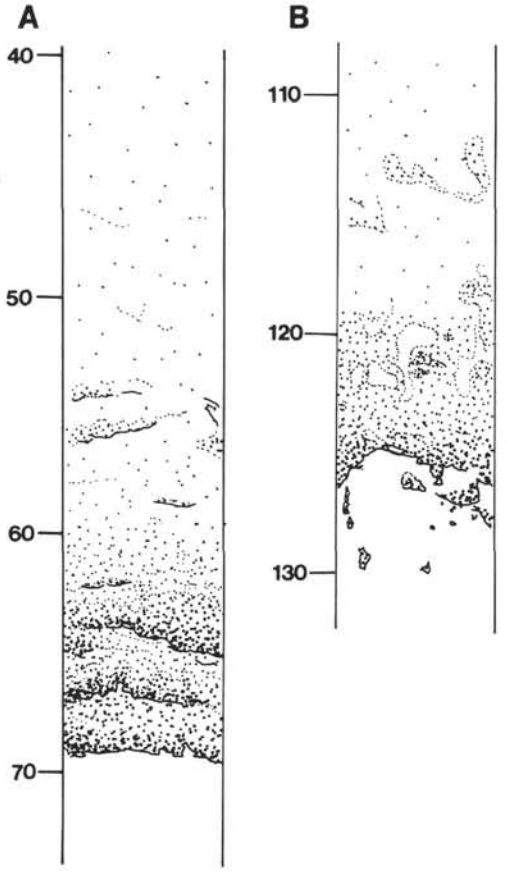

Figure 4. Sketches of ash layers in Section 136-842A-1H-6. **A.** Interval 39–73 cm. **B.** Interval 107–132 cm.

gioclase, olivine, clinopyroxene, and opaque minerals (probably ilmenite). These volcaniclastics are, of course, enriched in the visible ash layers. Nonetheless, a very small amount of volcaniclastics is scattered in every sample shallower than 10 mbsf in each hole.

Most volcaniclastic-enriched ash layers include significant amounts of fine-grained sediments. Most of these volcaniclastic grains are supported within a clay- and fine-silt-size matrix. Hole 842B was the only one to penetrate below 10 mbsf, where some visible ash layers exist. The majority of volcanic glasses between 10 and 18 mbsf have been altered to clay minerals, sometimes making it difficult to distinguish them from matrix clay in thin sections. Other volcaniclastics such as olivine, pyroxenes, and feldspar remain unaltered (Pl. 1, Fig. 3). Below 18 mbsf zeolitic (phillipsite?) clay was found. The dominant materials are pelagic clays in most samples. Siliceous biogenic materials such as radiolarians and diatoms are common in some samples. Carbonaceous biogenic materials, mostly nannofossils and foraminifers, are observed within and below the ash layer (Interval 136-842A-1H-6, 120–126 cm). In most samples, small, usually spherical forms of dark brownish opaque materials are observed. These opaque materials are probably the "red brown semiopaque oxide" described in Yeats, Hart, et al. (1976).

Grain-Size Analysis

Grain size was measured for all samples, and the results are shown in Table 2. Fine-silt-size particles are the dominant fraction in most samples. Coarse grains are prominent in visible ash layers. Sand-size modal peaks are only recognized in the visibly well-preserved ash layers. However, grain-size distributions show poor sorting and fine tails in all the ash-layer samples. No sand-size modal peak was found in the heavily bioturbated ash-layer samples, which include comparatively large amounts of sand-size volcaniclastics (Fig. 5). Figure 6 indicates coarse silt- and sand-size particles are mostly volcaniclastics and siliceous fossils. For Samples 842A-1H-6, 67–68 cm, and -1H-6, 58–59 cm, we measured the length and width of 100 volcaniclastic

Table 2. Results of grain-size analysis.

Sample (cm)	842A-1H-2, 89–90	842A-1H-6, 42–43	842A-1H-6, 58–59	842A-1H-6, 67–68	842A-1H-6, 71–72	842A-1H-6, 119–120	842A-1H-6, 123–124	842A-1H-6, 127–128	842B-1H-1, 20–21	842B-1H-2, 19–20	842B-1H-2, 99–100
Mean (μm)	19.2	9.2	10.2	20.4	10.0	11.9	14.4	10.2	5.2	6.7	16.3
Mode (μm)	42.5	10.7	12.0	48.5	10.9	17.6	19.1	11.4	4.5	10.2	34.6
Sand (%)	1.6	0.0	0.0	10.2	0.4	0.1	0.8	0.7	0.0	0.0	1.7
Coarse silt (%)	23.5	5.9	5.6	27.5	9.8	9.4	15.1	11.8	0.0	0.4	23.7
Fine silt (%)	63.8	72.3	75.4	47.0	70.9	74.4	70.3	67.4	62.0	71.3	61.6
Clay (%)	19.1	21.8	19.0	15.4	18.9	16.1	13.8	20.1	38.0	28.3	13.0

Sample (cm)	842B-1H-3, 19–20	842B-1H-4, 20–21	842B-1H-4, 98–99	842B-2H-2, 98–99	842B-2H-3, 65–66	842B-2H-4, 2–3	842B-2H-5, 75–76	842B-2H-5, 88–89	842B-2H-5, 96–97	842B-2H-5, 133–134	842B-2H-5, 140–141
Mean (μm)	12.0	8.0	13.7	4.9	5.9	9.5	9.5	15.0	9.2	8.9	11.3
Mode (μm)	17.8	11.4	19.1	4.5	4.5	11.8	17.8	24.8	11.7	17.1	20.4
Sand (%)	1.1	0.0	0.9	0.0	0.0	0.0	0.0	0.2	0.0	0.0	0.0
Coarse silt (%)	15.8	0.9	15.8	0.0	0.7	2.1	2.0	16.2	1.4	1.0	8.7
Fine silt (%)	66.4	73.9	69.4	60.1	65.2	78.1	76.8	67.8	77.0	77.2	71.6
Clay (%)	16.6	25.2	13.9	39.1	34.1	19.8	21.2	15.7	21.6	21.8	19.7

Sample (cm)	842B-1H-4, 20–21	842B-3H-1, 24–25	842B-3H-1, 28–29	842B-3H-1, 64–65	842B-3H-2, 134–135	842B-3H-2, 141–142	842B-3H-3, 1–2	842B-3H-3, 42–43	842B-3H-4, 10–11	842B-4H-5, 3–4	842B-4H-5, 9–10
Mean (μm)	7.9	11.4	9.4	7.5	5.2	7.9	9.7	4.0	3.9	3.7	3.9
Mode (μm)	4.7	22.6	19.3	10.6	4.4	11.0	11.7	4.2	4.2	4.0	4.1
Sand (%)	0.0	0.2	0.0	0.0	0.0	0.0	0.0	0.0	0.0	0.0	0.0
Coarse silt (%)	4.0	13.5	8.1	3.8	0.4	0.4	6.7	0.0	0.0	0.0	0.0
Fine silt (%)	70.2	67.7	69.2	68.6	60.9	75.2	72.4	50.2	48.8	44.7	48.3
Clay (%)	25.8	18.6	22.7	27.6	38.7	24.4	20.9	49.8	51.2	55.3	51.7

Sample (cm)	842B-4H-5, 16–17	843C-1H-1, 24–25	843C-1H-1, 40–41	843C-1H-2, 58–59	843C-1H-2, 97–98	843C-1H-2, 136–137	843C-1H-3 27–28	843C-1H-3 66–67
Mean (μm)	3.7	5.4	7.5	7.8	13.7	17.4	19.2	11.1
Mode (μm)	4.0	4.5	10.6	10.9	20.6	20.4	35.9	11.2
Sand (%)	0.0	0.0	0.0	0.0	1.3	4.5	4.8	1.1
Coarse silt (%)	0.0	0.0	4.3	0.7	20.8	23.0	26.2	15.6
Fine silt (%)	44.8	62.8	68.9	74.6	63.9	61.2	57.6	64.6
Clay (%)	55.2	37.2	27.8	24.7	14.9	11.2	11.4	18.8

Note: Sand = >63 μm, coarse silt = 31–63 μm; fine silt = 4–31 μm; clay = <4 μm.

particles in thin section. No significant difference in type, length, and width among volcaniclastic particles was found (Table 3). These grain-size analyses reveal a tendency for the median and modal diameters to increase as depth decreases (Fig. 7).

Reflective Index of Basaltic Glasses

Fourteen samples included enough fresh glass shards (sideromelane) to measure the reflective index (Table 4). The indices of these glasses range between 1.585 and 1.606. They have basaltic compositions (Schmincke, 1981) and are similar to Site 311 glass samples (Larson, Moberly, et al., 1975). We observed no significant differences in range or deviation of the reflective index with differences in degree of bioturbation and grain-size distribution.

It seems from observation of these samples representing three holes that glass shards between 2 and 6 mbsf have approximately 1.590 modal and mean values. The other glass shards have about 1.600 both above and below the interval of 2 to 6 mbsf (Fig. 8). Based on the reflective index, the glass shards around 2.5 mbsf may be correlated between Holes 842B and 843C.

DISCUSSION

Hole 842B is the only hole to penetrate below 10 mbsf. Most glasses below 10 mbsf have altered to clay minerals or zeolite, and not enough fresh basaltic glass shards were found to measure the reflective index. Therefore, the following discussion is based primarily on samples from the three holes shallower than 10 mbsf.

Source Area of Volcaniclastic Fragments

The shapes of most fresh glasses are very similar to hydrovolcanic eruption products (Heiken and Wohletz, 1985). However, these glass fragments include various types of hydrovolcanic products (types 1, 2, 3, and 4 of Wohletz, 1983) and scoriaceous fragments. Moreover, these volcaniclastics include a significant amount of tachylite. Fisher and Schmincke (1984) mentioned that vesicular tachylite is one of the indicators of comparatively slow cooling (subaerial).

Composite sedimentary bodies composed of hyaloclastite, pillow lava, and subaerial lava are formed at the surf zone when subaerial basaltic lava flows enter the sea (Jones and Nelson, 1970; Furnes and Fridleifsson, 1974; Moore et al., 1973; Furnes and Sturt, 1976). Kokelaar (1986) mentioned that type 1 (hyaloclastite) pyroclast is produced under this condition, and types 3 and 4 pyroclast and scoria are produced by littoral cone-building explosions. Therefore, the probable formation area of such mixtures of various types of volcaniclastics is a littoral zone.

Transportation Process

Visible ash layers include pelagic clay and planktonic, mainly siliceous fossils, but others are essentially volcanic products. Most of these volcaniclastics are very angular in shape. Normal grading is the

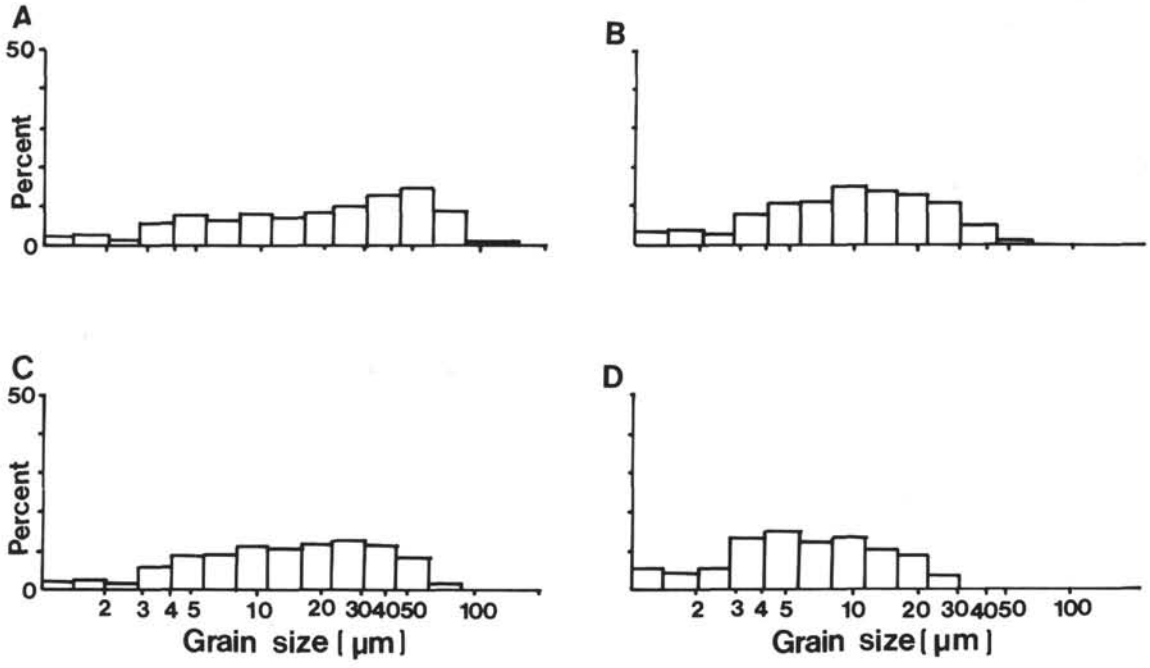

Figure 5. Examples of grain-size distribution of some samples. **A.** Sand-size, volcaniclastic-rich, well-bedded ash layer (Sample 136-842A-1H-6, 67–68 cm). **B.** Fine-grained part of well-bedded preserved ash layer (Sample 136-842A-1H-6, 58–59 cm). **C.** Ash layer heavily disturbed by bioturbation (Sample 136-843C-1H-2, 97–98 cm). **D.** Brown clay (Sample 136-843C-1H-1, 24–25 cm).

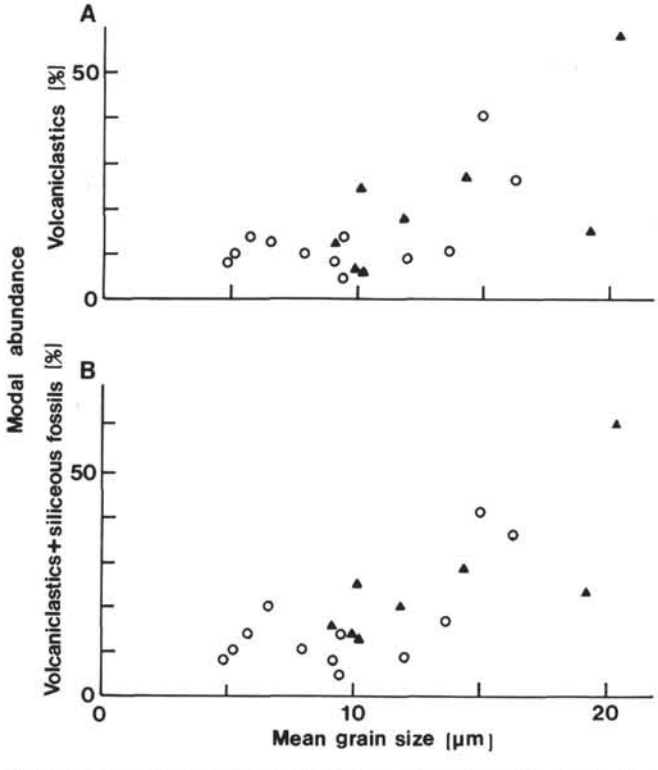

Figure 6. Relationships between grain size and percentage of volcaniclastics (**A**) and grain size and percentage of volcaniclastics and siliceous fossils (**B**). Solid triangle = Hole 842A; open circle = Hole 842B.

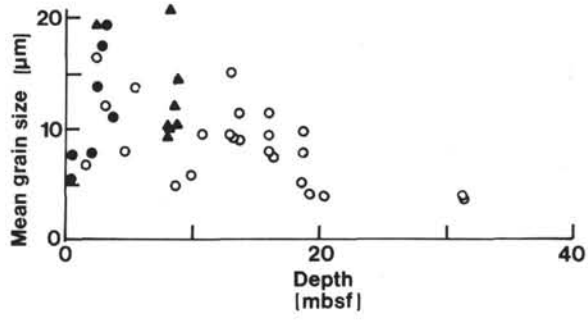

Figure 7. Vertical variations (in mbsf) of mean grain size (in microns). Solid triangle = Hole 842A; open circle = Hole 842B; solid circle = Hole 843C.

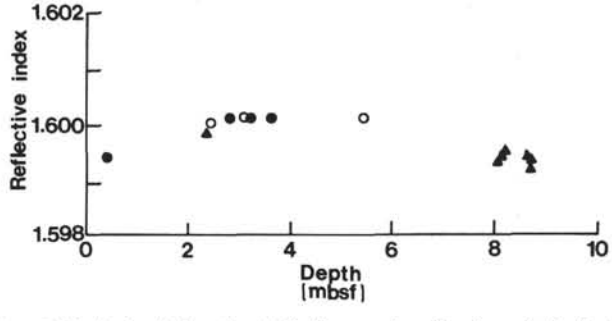

Figure 8. Vertical variations (in mbsf) of mean values (in microns) of reflective index of glass shards. Solid triangle = Hole 842A; open circle = Hole 842B; solid circle = Hole 843C.

Table 3. Length and width of volcanic fragments of Samples 136-842A-1H-6, 67–68 cm, and -1H-6, 58–59 cm, from grain-size measurements.

	Mean length (μ)	Mean width (μ)	Width/length (mean)	Number of grains
Sample 136-842A-1H-6, 58–59 cm				
Glass	34.17	18.13	0.55	36
Basaltic fragments	39.08	21.85	0.60	27
Plagioclase	29.82	14.82	0.51	15
Olivine	27.27	18.18	0.67	11
Pyroxene	52.25	33.08	0.62	3
Opaque minerals	18.75	10.63	0.56	8
Sample 136-842A-1H-6, 67–68 cm				
Glass	66.74	35.53	0.54	33
Basaltic fragments	94.09	55.53	0.70	33
Plagioclase	73.75	50.42	0.67	12
Olivine	64.38	39.69	0.62	8
Pyroxene	145.00	41.25	0.45	2
Opaque minerals	83.41	50.91	0.65	11

Note: 100 grains were measured on polished thin-section surfaces.

only distinct internal sedimentary structure of these ash layers. According to Huang (1980), two possible transportation processes may exist. One scenario is pelagic settling of air-fall pyroclasts. A second possibility is volcaniclastic materials transported to the present position by gravity currents (volcaniclastic turbidite).

The ash in these three holes includes mostly fine-grained volcaniclastics (mostly less than silt size), in which the settling velocity in the water column is controlled by Stokes' Law. These volcaniclastics include materials of different density such as heavy minerals (olivine and pyroxene), light minerals (plagioclase), and glasses. If ash layers are air-fall deposits, these volcaniclastics have been sorted by density contrast as they sank within the water column. Moreover, many glass shards have vesicles and show bubble-wall shapes in which settling velocities are slower than blocky crystal particles (Fisher, 1964). Sampling intervals are not so dense within the ash layers, but no tendency appears for enrichment of heavy minerals in the lower part of graded beds or coarse-grained samples (Fig. 9).

If the eruption duration were long and the modal compositions of pyroclastics were not constant during the eruption, later ashes may be mixed with earlier ashes (Ledbetter and Sparks, 1979). Therefore, it is probable that these modal compositions were modified by this process.

In the Pacific Ocean, many volcaniclastic turbidites and debris-flow deposits were collected by Deep Sea Drilling Project (DSDP) and ODP at the archipelagic apron of volcanic seamounts (Winterer, Ewing, et al. 1973; Larson, Moberly, et al., 1975; Kelts and McKenzie, 1976; Larson, Schlanger, et al., 1981; Moberly, Schlanger, et al., 1986; Lancelot, Larson, et al., 1990). DSDP Site 462 recovered thick Cretaceous volcaniclastic turbidites (Larson, Schlanger, et al., 1981), and ODP Site 802 (Lancelot, Larson, et al., 1990) recovered Miocene and Cretaceous volcaniclastic turbidites. The distance from the probable source area of these sites is greater than the distance between Oahu and Sites 842 and 843 (the Miocene deposit of Site 802 is 350 km from its source area). Even sand-size detritus can be carried by upslope flow of turbidity currents (Damuth and Embley, 1979). No distinct sedimentary structure was found except for normal-graded bedding within the ash layers at Sites 842 and 843. These observations suggest that these ash layers are a distal volcaniclastic turbidite. Large amounts of matrix pelagic clay in ash layers indicate mixing between volcaniclastics and pelagic clay by turbidity currents during transportation (Sparks and Wilson, 1983).

The majority of Cretaceous and Miocene archipelagic apron volcaniclastic turbidites are accompanied by shallow-water carbonate materials (Kelts and Arthur, 1981; Whitman et al., 1986; Lancelot, Larson, et al., 1990). These turbidites may include shallow-water or subaerial volcaniclastics. The Hawaiian Islands are fringed by coral reefs, but samples from Sites 842 and 843 do not include shallow-water carbonate fragments. However, calcareous materials are found at Site 311, south of Midway Island (Larson, Moberly, et al., 1975). The shallow-water carbonates at Sites 842 and 843 have been dissolved, as the sedimentation rate is low compared with other archipelagic apron areas. On the other hand, Fornari et al. (1979) reported a landslide body that is essentially composed of volcaniclastics from the surf zone where volcaniclastic productivity is high on the south flank of the island of Hawaii. Therefore, it is also probable that these ash layers were originally free or almost free of shallow-water carbonate fragments.

Disturbance of Bioturbation

We observed some degree of bioturbation disturbance even in visible ash layers. An ash layer in Sample 136-842A-1H-6, 63–70 cm, has a sharp bottom surface; this sample shows a sand-size modal peak (Fig. 5A). However, other visible ash layers show poorly sorted grain-size distribution (Fig. 5C). These characteristics indicate that the ash layers were mixed with ambient pelagic brown clays. Moreover, sand- or coarse silt-size volcaniclastic particles can be observed in most samples shallower than 10 mbsf. These volcaniclastics were probably dispersed by bioturbation from lower horizons.

The sedimentation rates among these three holes are similar (Dziewonski, Wilkens, Firth, et al., 1992). If the degree of disturbance from bioturbation is similar among these three holes, there should be a correlating ash layer in the case of air-fall ash. However, we observed no visible correlative ash layer among Holes 842A, 842B, and 843C. Sparks et al. (1984) showed that ash-layer disturbance depends on the sedimentation rate, hence the original thickness of ash layers is significantly different among these holes. The distance between Holes 842A and 842B is small, which indicates that these ash layers were not deposited by a simple air-fall process.

As Kelts and Arthur (1981) noted, the archipelagic apron around volcanic island volcaniclastic turbidites formed within a short period after the volcanic activity. Therefore, if these volcaniclastic sediments from Sites 842 and 843 are of turbidite origin, these ashes preserve the volcanic activity sequence. Of course, if these ashes were air-fall deposits, the succession represents a change in composition of erupted magma of the Hawaiian volcanoes. As mentioned in Ruddiman and Glover (1972), the degree of disturbance of bioturbation decreases exponentially, suggesting that volcanic glasses probably were not dispersed to any great extent after deposition, and the three horizons of reflective indices indicate the change in composition of erupted magma of the Hawaiian volcanoes.

SUMMARY

Three volcaniclastics (ash)-bearing sediment cores were collected during Leg 136. The sources of these volcaniclastics could be the volcanoes of the Hawaiian Islands. However, the occurrence and amount of volcaniclastics among these three cores are different. All ash layers show disturbance resulting from bioturbation. It appears that the effect of bioturbation is the most significant reason for these different ash layers. Two probable transportation processes may exist. One is air-fall pyroclastics produced by hydrovolcanism and settled in a pelagic environment. The other is turbidite coming primarily from the surf zone. The simple air-fall origin is unlikely because no correlative visible ash layers among these three holes exists. Therefore, turbidite transport is the favored explanation of the origin.

ACKNOWLEDGMENTS

We acknowledge Professor Yujiro Ogawa of the University of Tsukuba and Dr. Wonn Sho of Shizuoka University for their critical reviews of this manuscript. Part of the analysis of sediments was made

at the Ocean Research Institute of University of Tokyo. We also acknowledge Professor Asahiko Taira and Dr. Hidekazu Tokuyama for their helpful guidance and discussions.

REFERENCES*

Brocher, T.M., and ten Brink, U.S., 1987. Variations in oceanic Layer 2 elastic velocities near Hawaii and their correlation to lithospheric flexure. *J. Geophys. Res.,* 92:2647–2661.

Damuth, J.E., and Embley, R.W., 1979. Upslope flow of turbidite currents on the northwest flank of the Ceara Rise: western Equatorial Atlantic. *Sedimentology,* 26:825–834.

Danhara, T., Yamashita, T., Iwano, H., and Kasuya, M., 1992. An improved system for measuring refractive index using the thermal immersion method. *Quat. Int.,* 13/14:89–91.

Dziewonski, A., Wilkens, R., Firth, J., et al., 1992. *Proc. ODP, Init. Repts.,* 136: College Station, TX (Ocean Drilling Program).

Fisher, R.V., 1965. Settling velocity of glass shards. *Deep-Sea Res. Part A,* 12:345–353.

Fisher, R.V., and Schmincke, H.-U., 1984. *Pyroclastic Rocks:* New York (Springer-Verlag).

Fornari, D.J., Moore, J.G., and Calk, L., 1979. A large submarine sand-rubble flow on Kilauea volcano, Hawaii. *J. Volcanol. Geotherm. Res.,* 5:239–256.

Furnes, H., and Fridleifsson, I.B., 1974. Tidal effects on the formation of pillow lava/hyaloclastite deltas. *Geology,* 4:381–384.

Furnes, H., and Sturt, B.A., 1976. Beach/shallow marine hyaloclastite deposits and their geological significance—an example from Gran Canaria. *J. Geol.,* 84:439–453.

Hamilton, E.L., 1957. Marine geology of the southern Hawaiian ridge. *Geol. Soc. Am. Bull.,* 66:1011–1026.

Heiken, G., and Wohletz, K., 1985. *Volcanic Ash:* Berkeley (Univ. of California Press).

Huang, T.C., 1980. A volcanic sedimentation model: implications of processes and responses of deep-sea ashes. *Mar. Geol.,* 38:103–122.

Jones, J.G., and Nelson, P.H.H., 1970. The flow of basalt from air into water: its structural expression and stratigraphic significance. *Geol. Mag.,* 107:13–21.

Kelts, K., and Arthur, M.A., 1981. Turbidites after ten years of deep-sea drilling—wringing out the mop? *In* Warme, J.E., Douglas, R.G., and Winterer, E.L. (Eds.), *The Deep Sea Drilling Project: A Decade of Progress.* Spec. Publ.—Soc. Econ. Paleontol. Mineral., 32:91–127.

Kelts, K., and McKenzie, J.A., 1976. Cretaceous volcanogenic sediments from the Line Island chain: diagenesis and formation of K-feldspar, DSDP Leg 33, Hole 315A and Site 316. *In* Schlanger, S.O., Jackson, E.D., et al., *Init. Repts. DSDP,* 33: Washington (U.S. Govt. Printing Office), 789–831.

Kokelaar, B.P., 1986. Magma-water interactions in subaqueous and emergent basaltic volcanics. *Bull. Volcanol.,* 48:275–290.

Lancelot, Y., Larson, R., et al., 1990. *Proc. ODP, Init. Repts.,* 129: College Station, TX (Ocean Drilling Program).

Larson, R.L., Moberly, R., et al., 1975. *Init. Repts. DSDP,* 32: Washington (U.S. Govt. Printing Office).

Larson, R.L., Schlanger, S.O., et al., 1981. *Init. Repts. DSDP,* 61: Washington (U.S. Govt. Printing Office).

Ledbetter, M.T., and Sparks, R.S.J., 1979. Duration of large-magnitude explosive eruptions deduced from graded bedding in deep-sea ash layers. *Geology,* 7:240–244.

Moberly, R., Schlanger, S.O., et al., 1986. *Init. Repts. DSDP,* 89: Washington (U.S. Govt. Printing Office).

Moore, J.G., Phillips, R.L., Grigg, R.W., Peterson, D.W., and Swanson, D.A., 1973. Flow of lava into the sea, 1969–1971, Kilauea volcano, Hawaii. *Geol. Soc. Am. Bull.,* 84:537–546.

Ruddiman, W.F., and Glover, L.K., 1972. Vertical mixing of ice-rafted volcanic ash in north Atlantic sediments. *Geol. Soc. Am. Bull.,* 83:2817–2836.

Schmincke, H.-U., 1981. Ash from vitric muds in deep sea cores from the Mariana Trough and fore-arc regions (south Philippine Sea) (Sites 453, 454, 455, 458, 459), Deep Sea Drilling Project, Leg 60. *In* Hussong, D.M., Uyeda, S., et al., *Init. Repts. DSDP,* 60: Washington (U.S. Govt. Printing Office), 473–481.

Sparks, R.S.J., Brazier, S., Huang, T.C., and Muerdter, D., 1984. Sedimentology of the Minoan deep-sea tephra layer in the Aegean and eastern Mediterranean. *Mar. Geol.,* 54:131–167.

Sparks, R.S.J., and Wilson, C.N.J., 1983. Flow-head deposit in ash turbidites. *Geology,* 11:348–351.

Whitman, J.M., Baltuck, M., Haggerty, J.A., and Dean, W., 1986. Turbidite sedimentology and history of the East Mariana Basin. *In* Moberly, R., Schlanger, S.O., et al., *Init. Repts. DSDP,* 89:365–388.

Winterer, E.L., Ewing, J.I., et al., 1973. *Init. Repts. DSDP,* 17: Washington (U.S. Govt. Printing Office).

Wohletz, K.H., 1983. Mechanisms of hydrovolcanic pyroclast formation: grain size, scanning electron microscopy, and experimental studies. *J. Volcanol. Geotherm. Res.,* 17:31–63.

Yeats, R.S., Hart, S.R., et al., 1976. *Init. Repts. DSDP,* 34: Washington (U.S. Govt. Printing Office).

* Abbreviations for names of organizations and publications in ODP reference lists follow the style given in *Chemical Abstracts Service Source Index* (published by American Chemical Society).

Date of initial receipt: 18 September 1992
Date of acceptance: 4 January 1993
Ms 136SR-207

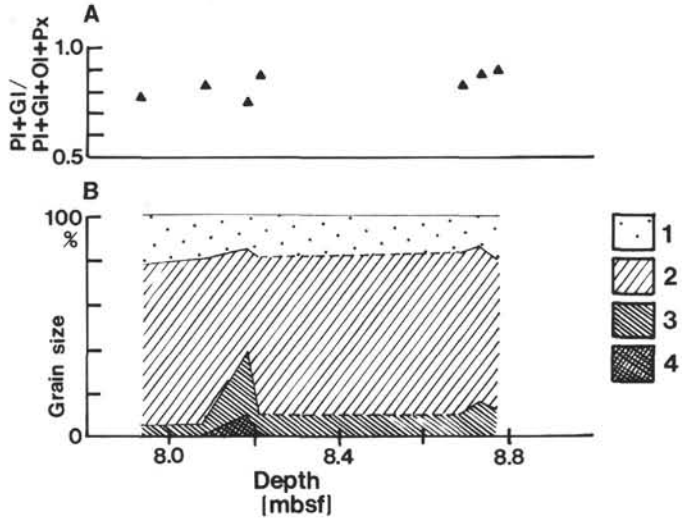

Figure 9. **A.** Variations in ratio of heavy (olivine and pyroxene) and light (plagioclase and glass) to light volcaniclastics. **B.** Grain size vs. depth. Horizontal axis of **A** is same as that for **B.** 1 = clay; 2 = fine silt; 3 = coarse silt, 4 = sand.

Table 4. Results of reflective index analysis of basaltic volcanic glasses.

Sample (cm)	842A-1H-2, 89–90	842A-1H-6, 58–59	842A-1H-6, 67–68	842A-1H-6, 71–72	842A-1H-6, 119–120	842A-1H-2, 123–124	842A-1H-6, 127–128	842B-1H-2, 99–100	842B-1H-3, 19–20	842B-1H-4, 98–99	843C-1H-1, 40–41	843C-1H-2, 58–59	843C-1H-2, 138–139	843C-1H-3, 66–67
Maximum	1.606	1.600	1.605	1.603	1.606	1.603	1.604	1.605	1.608	1.606	1.601	1.609	1.606	1.608
Minimum	1.587	1.588	1.587	1.588	1.586	1.586	1.586	1.589	1.596	1.587	1.587	1.596	1.597	1.592
Mean	1.598	1.593	1.594	1.595	1.594	1.592	1.593	1.600	1.601	1.601	1.594	1.601	1.601	1.601
Standard deviation	0.004	0.003	0.004	0.004	0.005	0.004	0.005	0.003	0.003	0.004	0.003	0.003	0.002	0.004

Note: 30 grains were measured for each sample.

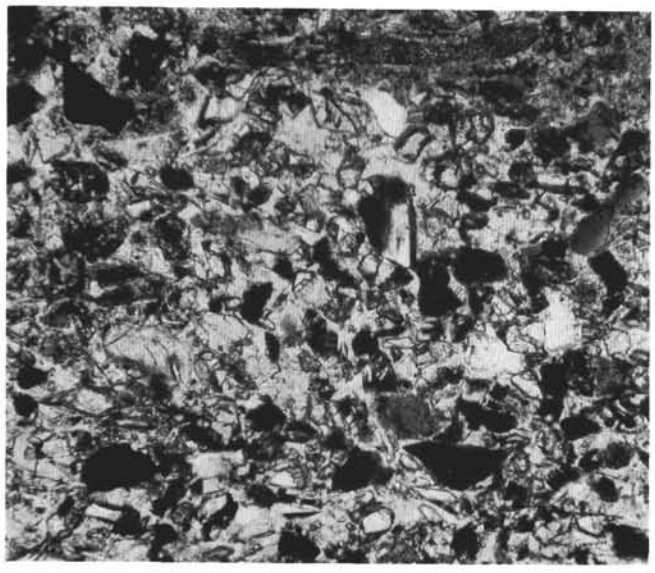

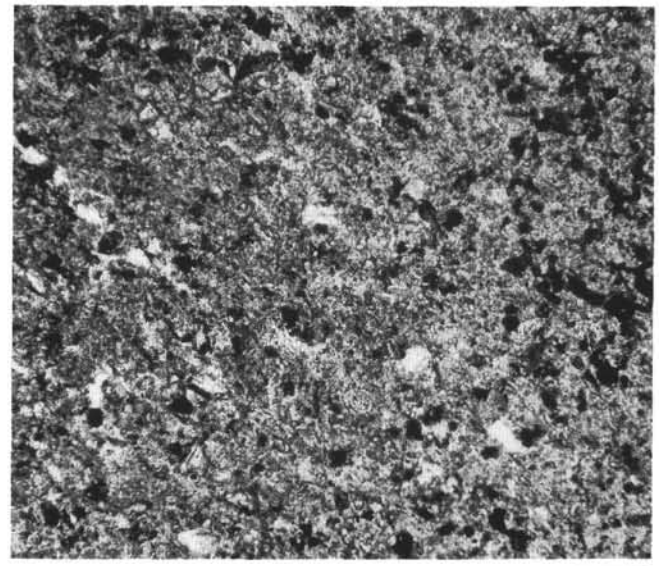

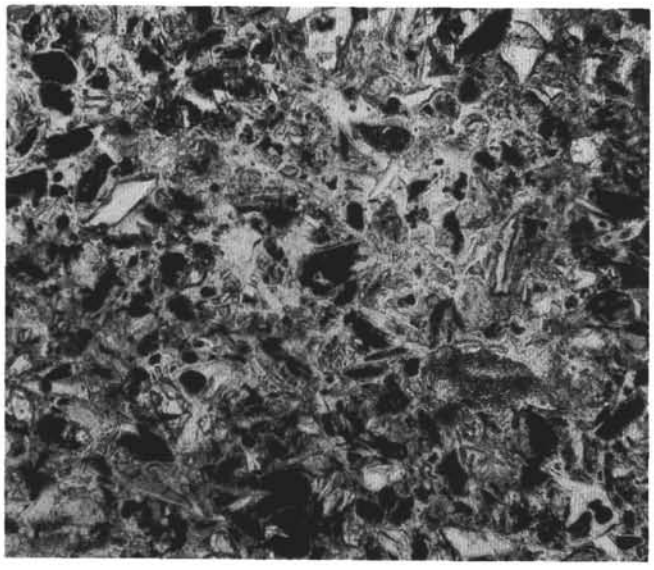

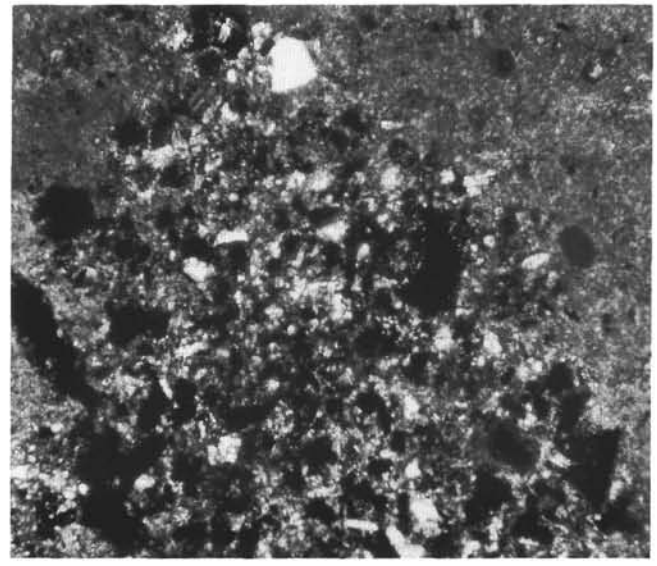

Plate 1. Thin-section microphotographs. **1.** Sand-size volcaniclastic-rich ash layer (Sample 136-842A-1H-6, 67–68 cm). **2.** Fine-grained volcaniclastic ash layer (Sample 136-842A-1H-6, 58–59 cm). **3.** Altered glass-rich ash layer (Sample 136-842B-2H-5, 89–90 cm). **4.** Sand-size volcaniclastic-filled pod in clay (Sample 136-842A-1H-6, 127–128 cm).

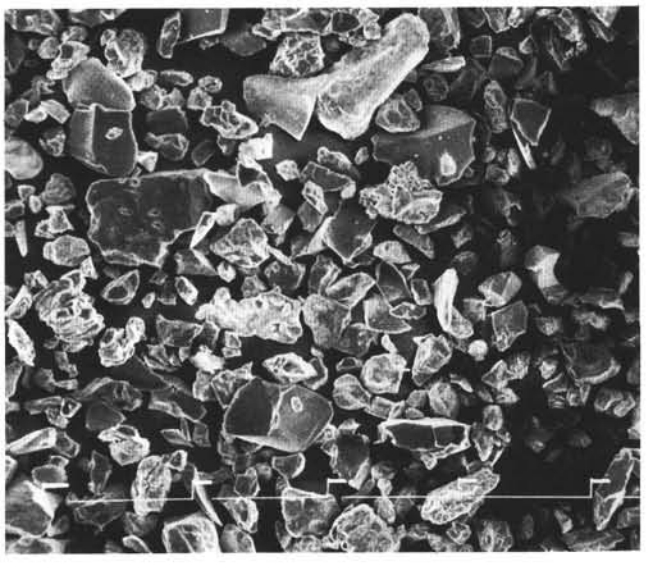

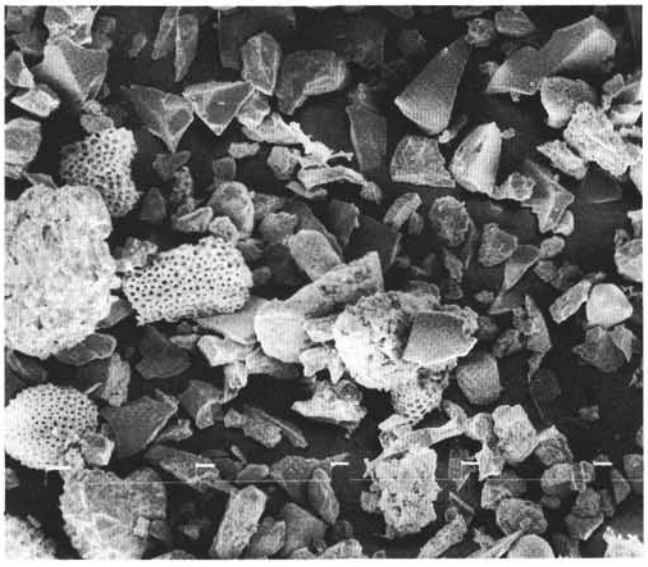

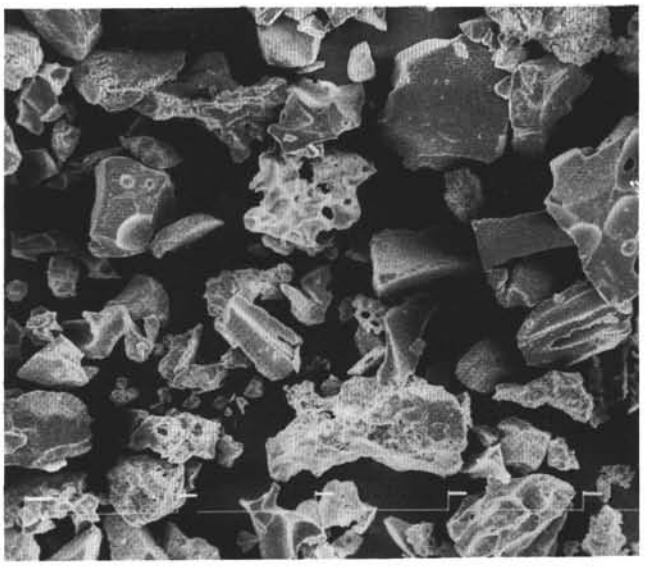

Plate 2. SEM microphotographs of coarse fractions. **1.** Sample 136-842A-1H-6, 58–59 cm. **2.** Sample 136-842A-1H-6, 67–68 cm. **3.** Sample 136-842A-1H-6, 71–72 cm. **4.** Sample 136-843C-1H-2, 136–137 cm.

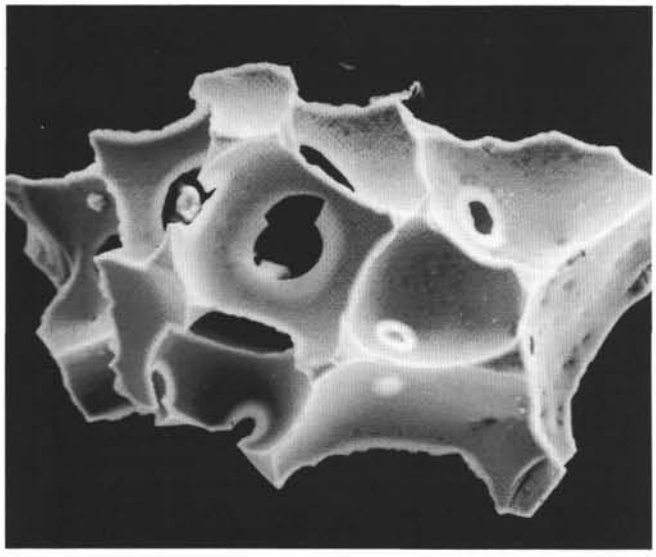

1

0.01 mm

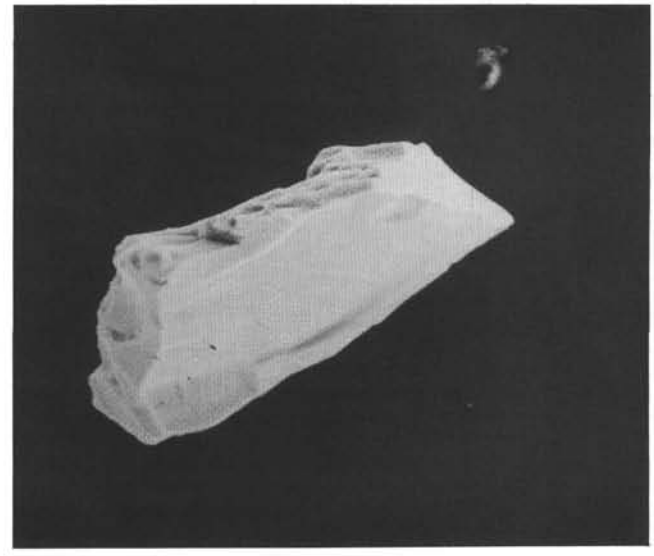

2

0.01 mm

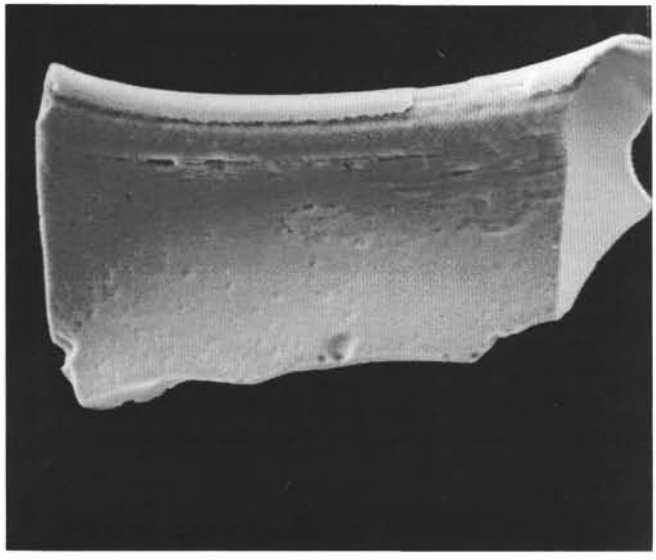

3

0.01 mm

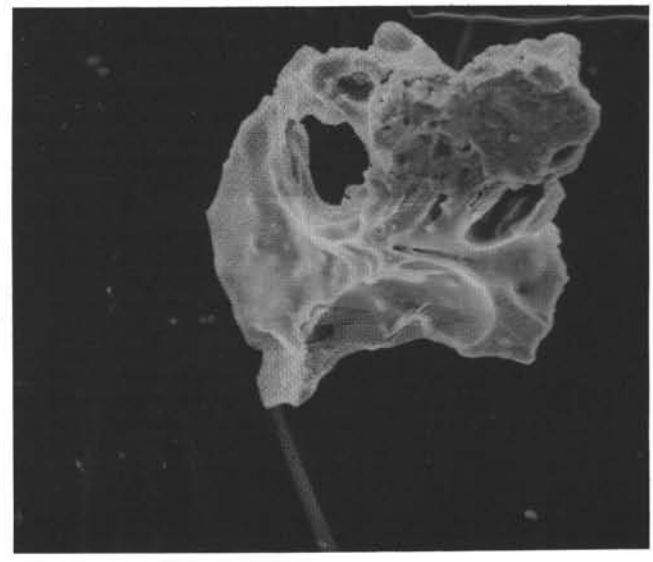

4

0.01 mm

Plate 3. SEM microphotographs of volcanic glass shards. **1.** Scoriaceous fragment in Sample 136-843C-1H-2, 136–137 cm. **2.** Blocky-shaped fragment in Sample 136-843C-1H-1, 40–41 cm. **3.** A fragment in Sample 136-842A-1H-6, 123–124 cm. **4.** Moss-like fragment in Sample 136-843C-1H-3, 27–28 cm.